10 Response of Buried Continuous Pipelines to Wave Propagation

There have been some events, such as the 1964 Puget Sound, 1969 Santa Rosa, 1983 Coalinga and 1985 Michoacan earthquakes, for which seismic wave propagation was the predominate hazard to buried pipelines. For example, the damage ratio for the water supply system in the Lake Zone (soft soil zone) of Metropolitan Mexico City of about 0.45 repairs/km has been attributed to wave propagation effects in the 1985 Michoacan event.

As discussed in Chapter 3, when a seismic wave travels along the ground surface, any two points located along the propagation path will undergo out-of-phase motions. Those motions induce both axial and bending strains in a buried pipeline due to interaction at the pipe-soil interface. For segmented pipelines, damage usually occurs at the pipe joints. Although seismic wave propagation damage to continuous pipelines is less common, the observed failure mechanism is typically local buckling.

This and the following chapter focus on buried pipe response due to wave propagation effects. The existing methods for evaluating the response of continuous pipelines as well as the behavior at elbows and tees are discussed and compared in this chapter. The following chapter discusses similar issues for segmented pipelines.

10.1 Straight Continuous Pipelines

In general, the axial strain induced in a straight continuous pipeline depends on the ground strain, the wavelength of the travelling waves and the interaction forces at the pipe-soil interface. For small to moderate ground motion, one may simply assume

that pipe strain is equal to ground strain. However, for large ground motion, slippage typically occurs at the pipe-soil interface, resulting in pipe strain somewhat less than the ground strain.

10.11 Newmark Approach

Simplified procedures for assessing pipe response due to wave propagation were first developed by Newmark (1967), and have since been used and/or extended by a number of authors (e.g., Yeh, 1974). Newmark's approach is based on three assumptions. The first assumption, which is common to most all the deterministic approaches, deals with the earthquake excitation. The ground motion (that is, the acceleration, velocity and displacement time histories) at two points along the propagation path are assumed to differ only by a time lag. That is, the excitation is modeled as a traveling wave. The second assumption is that pipeline inertia terms are small and may be neglected (Wang and M. O'Rourke, 1978). Experimental evidence from Japan (Kubo, 1974) as well as analytical studies (Sakurai and Takahashi, 1969, Shinozuka and Koike, 1979) indicate that this is a reasonable engineering approximation. The third assumption is that there is no relative movement at the pipe-soil interface and hence, the pipe strain equals the ground strain.

Figure 10.1 shows a pipeline subject to S-wave propagation in a vertical plane having an angle of incidence γ_s with respect to the vertical.

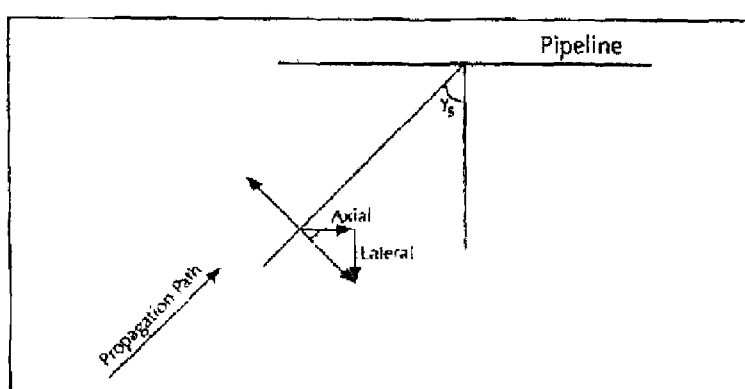

After Meyersohn, 1981

■ Figure 10.1 Pipeline Subject to S-wave Propagation

For this case, the ground strain parallel to the pipe axis is:

$$\varepsilon_g = \frac{V_m}{C_s} \sin\gamma_s \cos\gamma_s \qquad (10.1)$$

where V_m is the peak ground velocity and C_s is the shear wave velocity.

In terms of Equation 3.8, $V_m \cos\gamma_s$ is the ground velocity parallel to the pipe axis and, as noted in Equation 3.5, $C_s/\sin\gamma_s$ is the apparent propagation velocity with respect to the ground surface and the pipeline axis.

Similarly, for R-wave, the ground strain parallel to the pipe axis is.

$$\varepsilon_g = \frac{V_m}{C_{ph}} \qquad (10.2)$$

Since bending strain in a pipe due to wave propagation is typically a second order effect, our attention is restricted to axial strain in the pipe. Equations 10.1 and 10.2 overestimate pipe strain, especially when the ground strain is large. For those cases, slippage occurs at the pipe-soil interface and the pipe strain is less than the ground strain

10.1.2 Sakurai and Takahashi Approach

In relation to Newmark's assumption regarding pipeline inertia, Sakurai and Takahashi (1969) developed a simple analytical model for a straight pipeline surrounded by an infinite elastic medium (soil). They used D'Alembert's principle to handle the inertia force. For a pipeline subject to the ground displacement u_g, the equilibrium for the pipe segment is:

$$\rho \frac{\partial^2 u_p}{\partial t^2} - E \frac{\partial^2 u_p}{\partial z^2} = K_g (u_g - u_p) \qquad (10.3)$$

where u_p is the displacement of the pipeline in z direction (longitudinal direction), assumed to be the direction of wave propagation,

K_s is the linear soil stiffness per unit length as shown in Figure 5.2 and ρ is the mass density of pipe material.

The analytical results from Equation 10.3, which do not consider slippage at the pipe-soil interface, indicate that the pipe strain is about equal to free field strain and hence, the inertia effects are negligible. This result regarding inertia terms is not surprising in light of the fact that the unit weight of a fluid filled pipe is not greatly different from that of the surrounding soil.

10.1.3 Shinozuka and Koike Approach

In relation to Newmark's assumption regarding no relative displacement at the pipe-soil interface, Shinozuka and Koike (1979) modify Equation 10.3 as follows:

$$\rho \frac{\partial^2 u_p}{\partial t^2} - E \frac{\partial^2 u_p}{\partial z^2} = \tau_s / t \qquad (10.4)$$

where τ_s is the shear force at the pipe-soil interface per unit length and t is the pipe wall thickness.

Neglecting the effects of inertia, Shinozuka and Koike (1979) developed a conversion factor between ground and pipe strains. For the case of no slippage at the pipe-soil interface (i.e., the soil springs remain elastic), the conversion factor is,

$$\beta_0 = \frac{1}{1 + \left(\frac{2\pi}{\lambda}\right)^2 \cdot \frac{AE}{K_g}} \qquad (10.5)$$

That is, the pipe strain is β_0 times the ground strain. This result holds as long as the shear strain at the pipe-soil interface, γ_0,

$$\gamma_0 = \frac{2\pi}{\lambda} \frac{Et}{G} \varepsilon_g \beta_0 \qquad (10.6)$$

is less than the critical shear strain, γ_{cr}, beyond which slippage occurs at the pipe-soil interface. The critical shear strain as estimated by Shinozuka and Koike is:

$$\gamma_{cr} = \frac{t_u}{\pi DG} \tag{10.7}$$

In their analysis, Shinozuka and Koike (1979) assumed that the critical shear strain is 1.0×10^{-3}. That is, for $\gamma_0 \leq 1\times10^{-3}$, slippage will not take place, while for $\gamma_0 > 1\times10^{-3}$, slippage occurs at the pipe-soil interface.

For large amounts of ground movement, i.e., $\gamma_0 > \gamma_{cr}$, the ground to pipe conversion factor is:

$$\beta_c = \frac{\gamma_{cr}}{\gamma_o} q\beta_o \tag{10.8}$$

where q is a factor which range from 1 to $\pi/2$ and quantifies the degree of slippage at the pipe-soil interface. That is for slippage over the whole pipe length $q = \pi/2$.

The pipe axial strain is then simply calculated by:

$$\varepsilon_p = \beta_c \cdot \varepsilon_g \tag{10.9}$$

10.1.4 M. O'Rourke and El Hmadi Approach

Also in relation to Newmark's "no relative displacement assumption", M. O'Rourke and El Hmadi (1988) use a somewhat different approach to estimate the maximum axial strain induced in a continuous pipe due to wave propagation.

Consider a model of a buried pipeline shown in Figure 10.2. The pipe has cross-sectional area A and modulus of elasticity E. The soil's resistance to axial movement of the pipe is modeled by a linear spring with stiffness K_s and a slider which limits the soil spring force to the maximum frictional resistance t_u at the pipe-soil interface. If the system remains elastic, that is the pipe strain

remains below its yield strain and the soil spring force remains below t_u, the differential equation for the pipe axial displacement $U_p(x)$ is:

$$\frac{d^2}{dx^2}U_p(x) - \beta^2 U_p(x) = -\beta^2 U_g(x) \qquad (10.10)$$

where $\beta^2 = K_g/(AE)$ and $U_g(x)$ is the ground displacement parallel to the pipe axis.

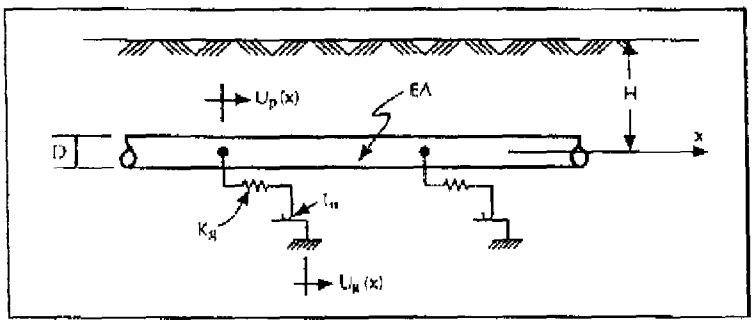

After M. O'Rourke and El Hmadi 1988

■ Figure 10.2 Continuous Pipeline Model

If the ground strain between two points separated by a distance L_s is modeled by a sinusoidal wave with wavelength $\lambda = 4L_s$, the ground deformation $U_g(x)$ (i.e., displacement of the base of the soil springs) is given by:

$$U_g(x) = \varepsilon_g L_s \sin\frac{\pi x}{2L_s} \qquad (10.11)$$

where ε_g is the average ground strain over a separation distance L_s.

The pipe strain is then given by:

$$\varepsilon_p = \frac{dU_p}{dx} = \frac{\pi}{2}\varepsilon_g \frac{\beta^2}{\beta^2 + \left(\frac{\pi}{2L_s}\right)^2}\cos\frac{\pi x}{2L_s} \qquad (10.12)$$

The elastic solution given in Equation 10.12 holds as long as the pipe strain is below its yield strain and the maximum force in the soil spring is less than the frictional resistance at the pipe-soil interface. That is,

$$\varepsilon_g L_s \left[1 - \frac{\beta^2}{\beta^2 + \left(\frac{\pi}{2L_s}\right)^2} \right] < \frac{t_u}{K_g} \qquad (10.13)$$

From Equation 10.13, a slip strain ε_s is defined as

$$\varepsilon_s = \frac{t_u}{K_g L_s} \left[\frac{\beta^2 + \left(\frac{\pi}{2L_s}\right)^2}{\left(\frac{\pi}{2L_s}\right)^2} \right] \qquad (10.14)$$

For moderately dense backfill, the slip strain is plotted in Figure 10.3 as a function of separation distance L_s. In this plot, two different nominal diameters of X-60 grade pipe, D = 30 cm (12in) and 91 cm (36 in), as well as two different burial depths, H = 0.75 m (2.5 ft) and 1.5 m (5 ft), are considered

Since the slippage strains are less than the strains which would results in pipe damage, propagation damage to continuous pipe typically involve some slippage at the pipe-soil interface.

With this in mind, M. O'Rourke and El Hmadi consider the upper bound case where slippage occurs over the whole pipe length. For a wave with wavelength λ, the points of zero ground strain (points A and B), as shown in Figure 10.4, are separated by a horizontal distance of λ/2. Assuming a uniform frictional force per unit length t_u, the maximum pipe strain at point C due to friction is given by:

$$\varepsilon_p = \frac{t_u L_s}{AE} \qquad (10.15)$$

where $L_s = \frac{\lambda}{4}$.

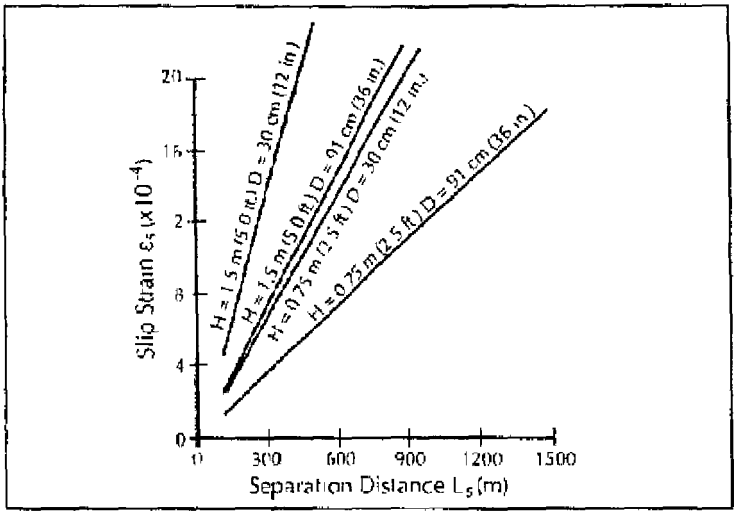

After M. O'Rourke and El Hmadi, 1988

■ Figure 10.3 Slip Strain vs. Separation Distance for Moderately Dense Sand Backfill

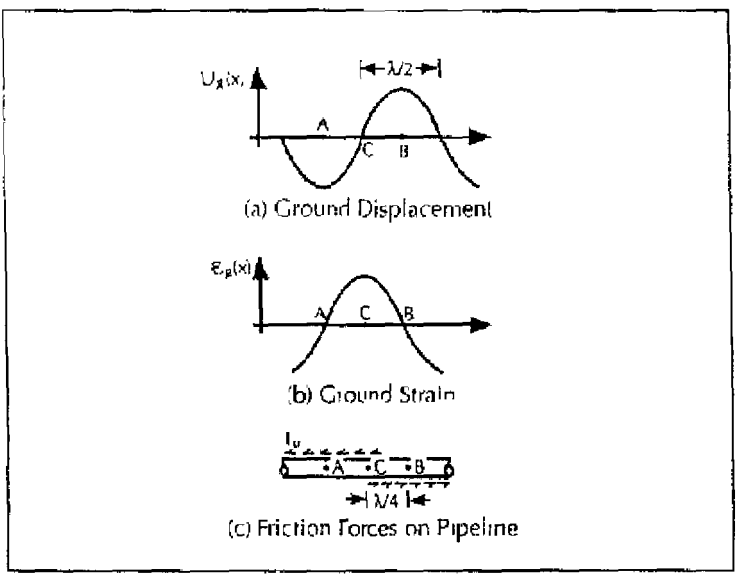

V. O'Rourke and El Hmadi, 1988

■ Figure 10.4 Friction Strain Model for Wave Propagation Effects on Buried Pipelines

For R-waves, M. O'Rourke and El Hmadi developed an analysis procedure to estimate the maximum pipe strain. This procedure compares axial strain in the soil to the strain in a continuous pipeline due to soil friction along its length. It is assumed that the soil strain is due to R-waves propagating parallel to the pipe axis. Due to the dispersive nature of R-wave propagation (i.e., phase velocity an increasing function of wavelength), the soil strain is a decreasing function of separation distance or wavelength. The pipe strain due to the friction at the pipe-soil interface is an increasing function of separation distance or wavelength. At a particular separation distance (that is, for a particular wavelength), the friction strain matches the soil strain. This unique strain then becomes the peak strain which could be induced in a continuous pipeline by R-wave propagation. Figure 10.5 shows both the ground strain and the pipe strain as function of the separation distance for an elastic pipe.

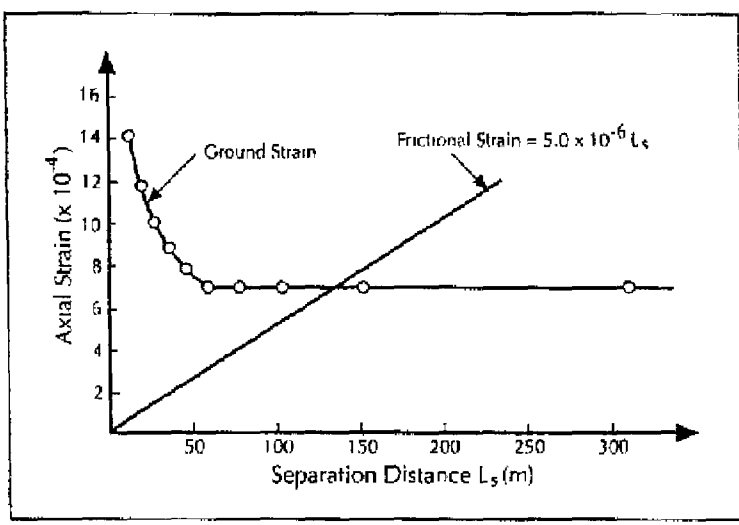

After M. O'Rourke and El Hmadi, 1988

■ Figure 10.5 Frictional Strain and Ground Strain vs. Separation Distance

As shown in Figure 10.5, for shorter quarter-wavelength separation distances, the pipeline frictional force acts over the whole length (i.e., from A to B in Figure 10.4) and hence, the pipe strain is linearly proportional to the quarter-wavelength separation dis-

tance. However, at longer quarter-wavelength separation distances, the pipe frictional force acting only near Points A and B results in a pipe strain equal to the ground strain at Point C. Note that this procedure for R-waves conservatively assumes that the peak ground velocity, V_{max}, applies to all frequencies (wavelengths) of R-wave propagation and that all frequencies (wavelengths) are present in the record.

10.1.5 COMPARISON AMONG APPROACHES

A comparison of the three approaches for a continuous pipe subject to wave propagation are presented in this subsection. The comparison is based on R-wave propagation having a dispersion curve with $\upsilon = 0.48$ shown in Figure 10.6. The peak particle velocity is taken as 0.35 m/s. The ground strains at three frequencies, from Equation 10.2, are presented in Table 10.1 along with the estimated strain in a straight pipeline with D=1.07 m (42 in) and t = 8 mm (5/16 in)

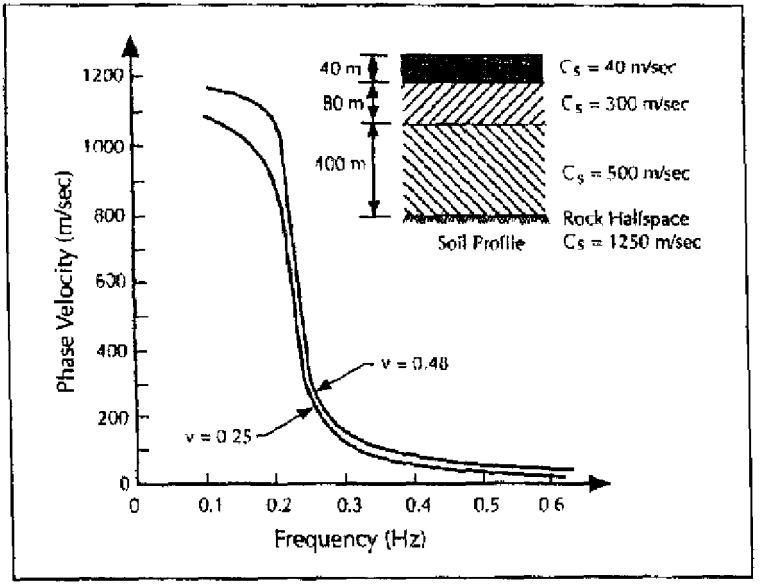

After M. O'Rourke and Ayala, 1990

■ Figure 10.6 Dispersion Curve and Ground Profile for the 1985 Mexico Earthquake Case History

■ Table 10.1 Comparison For Straight Continuous Pipeline

f (Hz)	C_{ph} (m/s)	Wavelength (m)	ε_g ($\times 10^{-3}$)	Pipe Strain ($\times 10^{-3}$)			
				Newmark	Shinozuka & Koike q=1	Shinozuka & Koike q=π/2	O'Rourke & El Hmadi
0.2	900	4500 m	0.39	0.39	0.31	0.39	0.39
0.3	137	456 m	2.5	2.5	0.77	1.3	1.3
0.4	92	230 m	3.8	3.8	0.4	0.6	0.6

As shown in Table 10.1, three approaches result in essentially the same pipe strain when the ground strain is small. In this case the pipe and soil move together and pipe strain is equal to ground strain since no slippage occurs. However, for large ground strains, the pipe strains from the Shinozuka and Koike approach as well as the M. O'Rourke and El Hmadi approach are both much less than ground strain. That is, although the ground strains are larger, the quarter wavelength distances over which the soil friction forces act are comparatively small. Note that Shinozuka and Koike's approach for full slippage case with $q = \pi/2$ is essentially the same as M. O'Rourke and El Hmadi's. For $q = 1$ in the Shinozuka and Koike approach, slippage occurs only over a portion of the pipe, and the corresponding pipe strains are lower bounds.

10.1.6 Comparison with Case Histories

During the 1985 Michoacan earthquake, a welded steel pipeline with $D = 107$ cm (42 in), $t = 0.8$ cm (5/16 in) and made of API 120 X-42 steel was damaged at several locations within the Lake Zone in Mexico City. As a case study, M. O'Rourke and Ayala (1990) estimated the compressive stress in the pipe due to R-wave propagation.

Figure 10.6 shows the dispersion curve for the fundamental R-wave, corresponding to the subsoil conditions of the Lake Zone in the Mexico City (M. O'Rourke and Ayala, 1990). Note that the generalized ground profile for this site consists roughly of a 40 m layer of soft clay with a shear wave velocity of 40 m/s. Under this layer, there are two stiffer strata with shear wave velocities of 300 and 500 m/s respectively. At the bottom is rock with a shear wave velocity of 1250 m/s.

For a pipe surrounded by loose sand with γ=110 lb/ft^3 (17.2 kN/m^3) and a coefficient of friction μ=0.5, the estimated compressive strain using M. O'Rourke and El Hmadi's procedure was about 0.002. The corresponding plot of the ground strain and friction strain is shown in Figure 10.7. Note in this figure, the friction strain is proportional to the quarter wavelength (i.e., separation distance) for strains less than about 0.001 ($\lambda/4 \approx 100$ m). For larger separation distances, although the axial force is still proportional to separation distance, the strain is not since we are now in the nonlinear portion of the stress-strain diagram for the steel. The local buckling strain is estimated to be about 0.0026 based upon D/t=134. That is, the analytical procedure suggests that the pipeline was very close to buckling. Note that the pipeline did, in fact, suffer a local buckling failure at several locations separated by distances of 300 to 500 m (984 to 1640 ft). This corresponds reasonably well with the 130 m (426 ft) quarter wavelength distance in Figure 10.7. That is, high compression regions are a wavelength apart, or 520 m (1706 ft) for the critical quarter-wavelength of 130 m (426 ft).

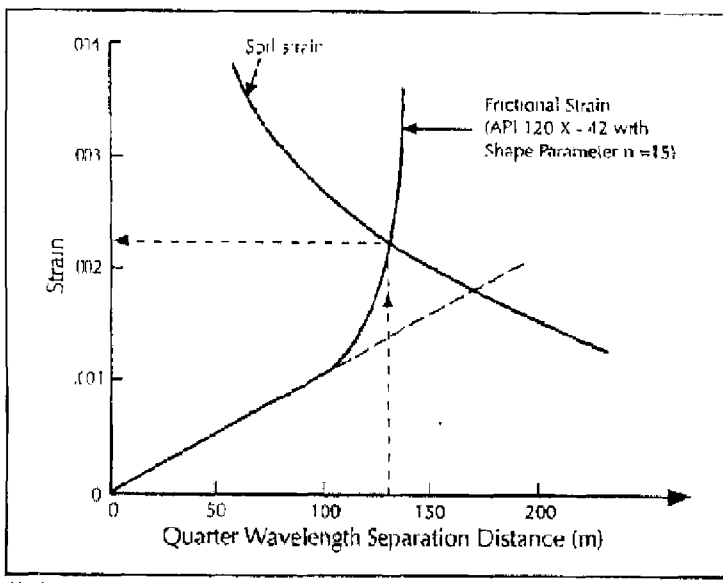

Allen M. O'Rourke and Ayala, 1990

■ Figure 10.7 Soil and Friction Strain for Ciudad Nezahualcoyotl Pipeline

BENDS AND TEES

A pipe network is typically composed of straight pipeline sections, and interconnecting bends, tees and crosses. The presence of these elements can produce additional bending strains at these interconnects and possibly lead to pipe damage. This section will focus on the effects of bends and tees.

10.2.1 SHAH AND CHU APPROACH

Considering the interaction forces at the pipe-soil interface, Shah and Chu (1974), as well as Goodling (1983), developed analytical formulae for forces and moment at elbows and tees. Figure 10.8 shows the forces acting on a pipeline and pipe deformation near the bend. The traveling wave is assumed to be propagating parallel to Element 1 with ground motion also parallel to Element 1 (e.g., R-waves). Element 2 is modeled as a beam on an elastic foundation with lateral soil stiffness K_s.

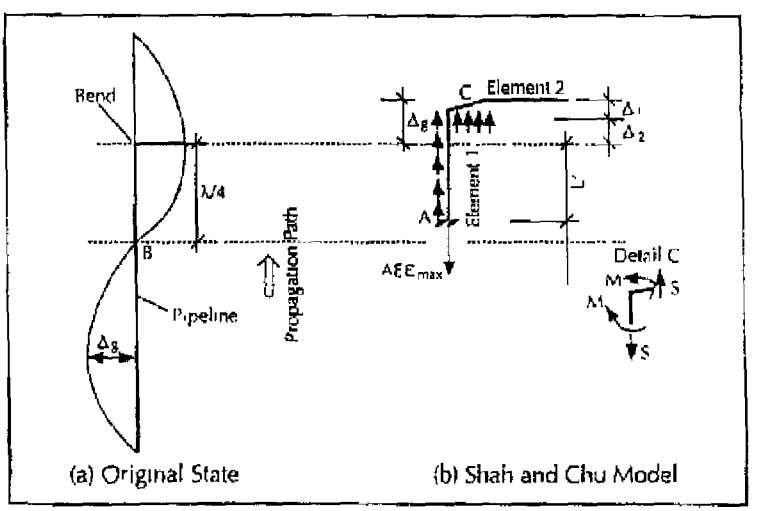

After Shah and Chu, 1974

■ Figure 10.8 Displacement and Forces in a Pipe with an Elbow

Shah and Chu (1974) assumed that the pipe and ground strains are equal at a location (Point A in Figure 10.8 b) where no relative displacement occurs at the pipe-soil interface. Denoting the distance from this location to the bend as L' shown in Figure 10.8, Shah and Chu (1974) as well as Goodling (1983) then estimated the maximum axial force in Element 1 at the bend (shear force in Element 2) by:

$$S = \varepsilon_{max} AE - t_u L' \tag{10.16}$$

The moment and flexural displacement at a bend can be then calculated as:

$$M = \frac{S}{3\zeta} \tag{10.17}$$

$$\Delta_T = \frac{4\zeta S}{3K_g} \tag{10.18}$$

where $\zeta = \sqrt[4]{K_g / (4EI)}$ and L' is the effective slippage length at the bend.

The effective slippage length, L', can be calculated based on displacement compatibility at the bend. That is, within the distance L', total ground deformation (taken as $\varepsilon_{max} L'$) is accommodated by the lateral displacement of Element 2, Δ_T, and axial deformation of Element 1, $\frac{SL'}{AE} + \frac{t_u L'^2}{2AE}$. For a long leg case (i.e., long Element 1), this compatibility condition yields,

$$L' = \frac{4AE\zeta}{3K_g}\left(\sqrt{1 + \frac{3\varepsilon_{max} K_g}{2t_u \zeta}} - 1\right) \tag{10.19}$$

Similarly, Figure 10.9 shows the forces and deformation for a tee, again for a wave propagating path parallel to Element 1.

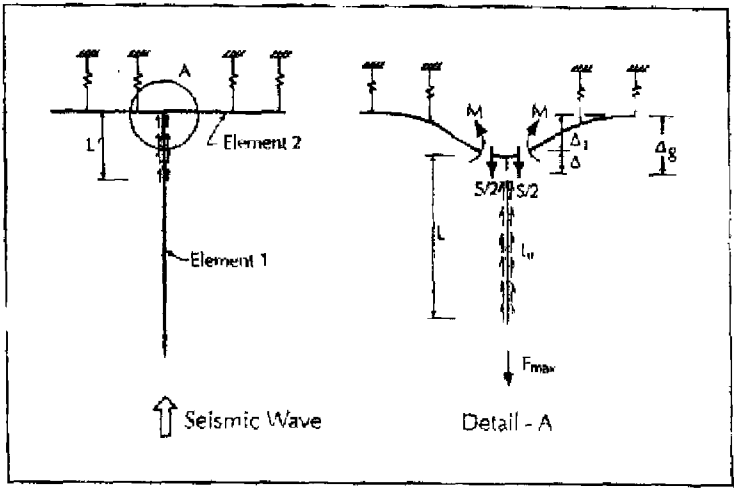

After Goodling, 1983

■ Figure 10.9 Representation of Forces, Moments and Displacement at a Tee

Using the same procedure as that for bends, Shah and Chu estimate the force, moment and displacement for a tee by the following equations:

$$S = \epsilon_{max} AE - t_u L' \tag{10.20}$$

$$M = \frac{S}{2\zeta} \tag{10.21}$$

$$\Delta_1 = \frac{5S}{K_g} \tag{10.22}$$

$$L' = \frac{AE\zeta}{2K_g}\left(\sqrt{1 + \frac{4\epsilon_{max}K_g}{t_u\zeta}} - 1\right) \tag{10.23}$$

Note that Shah and Chu (1974) as well as Goodling (1983) assume pipe strain is equal to the maximum ground strain at Point A (Figure 10.8). Based upon the previous discussion of straight pipe response to wave propagation, this assumption is likely only

true for small ground strains. Furthermore, they estimate the total ground displacement simply by the maximum ground strain times the effective length L'. This implies that the ground strain is constant over the length L' which only applies for a wavelength many times larger than the length L'.

10.2.2 Shinozuka and Koike Approach

Assuming a pipe moving with the soil at the location with zero ground movement (Point B in Figure 10.10), Shinozuka and Koike (1979) developed simple equations to estimate pipe strain at bends based on structural analysis similar to that discussed above. In their analysis, the effective length, that is, the L' term, is assumed to be a quarter wavelength, and the forces are obtained, as in the previous model, by displacement compatibility at the bend. The axial force, S, can be then expressed by:

$$S = \frac{3\lambda}{8\pi} \cdot \frac{K_g}{\zeta} \cdot \frac{1}{1+Q}(1-\beta_c)\varepsilon_g \qquad (10.24)$$

where $Q = \dfrac{3}{16}\dfrac{K_g \lambda}{AE\zeta}$.

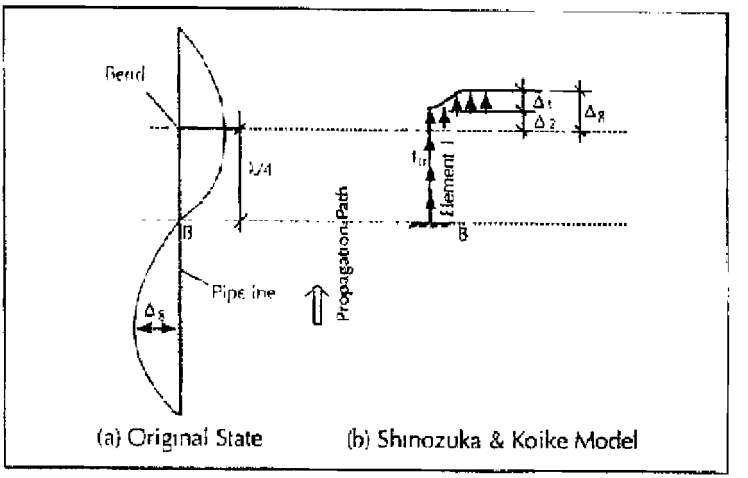

After Shinozuka & Koike 1979

■ Figure 10.10 Displacement and Forces in a Pipe at an Elbow

The moment and displacement at the bend can then be calculated by Equations 10.17 and 10.18. Note that the total ground deformation within the quarter wavelength is calculated by integrating the pipe strain. That is,

$$\Delta_g = \frac{\lambda}{2\pi}\,\varepsilon_{max} \tag{10.25}$$

Similarly, the axial force S in Element 1 for a tee is:

$$S = \frac{\lambda}{2\pi}\cdot\frac{K_g}{\zeta}\cdot\frac{1}{1+\frac{4}{3}Q}(1-\beta_r)\varepsilon_g \tag{10.26}$$

10.2.3 FINITE ELEMENT APPROACH

In order to independently evaluate the assumptions which underlay the existing approaches, the finite element model shown in Figure 10.11 was used. In this numerical model, axial and lateral soil springs are used to model the interaction at the pipe-soil interface. Element 1 is 600 m long and hence, considered appropriate for wavelength of roughly 600 m or less. The quasi-static seismic excitation is modeled by displacing the bases of the soil

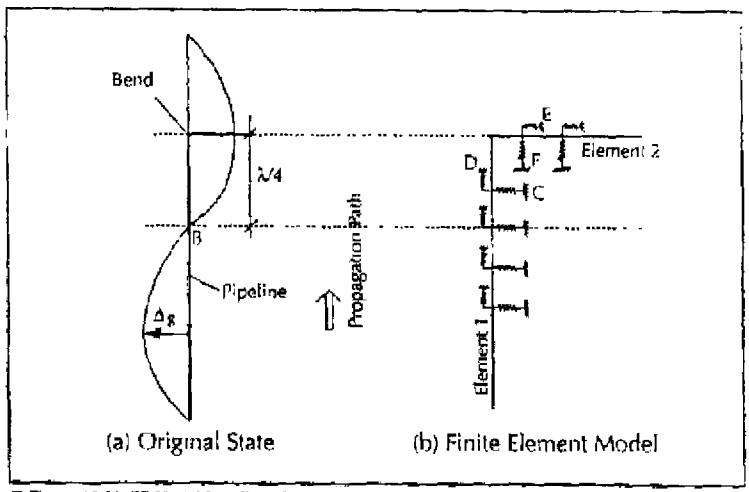

■ Figure 10.11 FE Model for Elbow Subject to Wave Propagation

springs. For example, point F moves Δ_g in the direction of wave propagation, while point E does not move. For Element 1, the movement of the bases (e.g., point D) of the longitudinal soil springs varies along the pipe matching the sinusoidal pattern as shown in Figure 10.11(a).

A steel pipe with diameter D = 0.76 m (30 in), wall thickness t = 0.0095 m (3/8 in) is considered. The assumed seismic excitation is an R-wave with V_{max} = 0.36 m/s propagating parallel to Element 1.

10.2.4 COMPARISON AMONG APPROACHES

Results from the finite element approach described in Section 10.2.3 are compared to the existing analytical approaches in this section. For an elbow, the force, moment and displacement at the elbow due to travelling wave effects are listed in Table 10.2 using the Shah and Chu approach, the Shinozuka and Koike approach as well as the finite element approach described above. Note that two cases are considered in Table 10.2. In this first case (Case I) the ground strain and wavelength are taken as 0.29×10^{-3} and 244 m respectively. While in Case II, $\varepsilon_g = 1.8\times10^{-3}$ and λ = 100 m.

From Equation 10.19, the effective length for the large ground strain, small wavelength case is 233.3 m by the Gooding/Shah and Chu approach. Since this effective length is much larger than a quarter wave length, that approach can not be used. Note that the effective length by Shinozuka and Koike matches relatively well with the finite element results for both cases considered here.

As shown in Table 10.2, for a small ground strain case, the peak pipe strain at the elbow by Shah and Chu is larger than that by both Shinozuka and Koike and the finite element method. This is due to the fact that Shah and Chu overestimate the ground deformation, and simply assume the maximum pipe strain equal to maximum ground strain. On the other hand, Shinozuka and Koike's approach underestimates the pipe strain at the elbow. This is due to the fact that the axial soil stiffness they suggested ($K_g = 2\pi C = 2\pi\rho C_s^2 = 4.1\times10^9$ N/m² (595 kips/in²)) is much larger than that ($K_g = t_u/x_u = 8.3\times10^6$ N/m² (1.2 kips/in²)) in the finite element model. For example, by using $K_g = 8.3\times10^6$ N/m² (1.2 kips/in²) in Shinozuka

and Koike's approach, for the small ground strain case, the peak strain at the elbow is estimated to be 4.9×10^{-5}, which matches the numerical strain (4.5×10^{-5}) very well

Overall, the comparison in Table 10 2 suggests that, of the available analytical approaches, the Shinozuka and Koike method appears more appropriate.

■ Table 10 2 Comparison For Bend

Approach	Case	λ (m)	ε_g ($\times10^{-3}$)	Effect Length (m)	Δ_g (cm)	Δ (cm)	S (N)	M (N·m)	Peak Strain
Goodling, Shah & Chu	II	244	0 29	42.8	1 24	0 61	4.2×10^{4}	5.9×10^{4}	1.4×10^{-4}
	I	100	1.8	233.3	-	-	-	-	-
Shinozuka & Koike	II	244	0 29	$61(\frac{\lambda}{4})$	1.1	001	71.8	100 6	0
	I	100	1 8	$25(\frac{\lambda}{4})$	2 9	2 4	1.64×10^{5}	2.3×10^{5}	5.5×10^{-4}
Finite Element	II	244	0 29	60	1 1	0.3	3.2×10^{4}	3.7×10^{4}	4.5×10^{-4}
	I	100	1.8	23 6	2 9	2.4	1.9×10	2.5×10^{5}	5.9×10^{-4}